Turbulence Generation in Homogeneous Particle-Laden Flows[*]

J.-H. Chen, J.-S. Wu[**] and G.M. Faeth
Department of Aerospace Engineering
The University of Michigan
Ann Arbor, Michigan 48109-2140

Abstract

Homogeneous turbulence generated by uniform fluxes of monodisperse spherical particles moving through a uniform flowing gas was studied. Measurements of phase velocities, moments, probability density functions, temporal power spectra and spatial integral scales were obtained using phase-discriminating laser velocimetry and particle sampling for counterflowing particle/air wind tunnel flows, to supplement earlier findings for particles falling in stagnant water and air. The combined data base involved particle Reynolds numbers of 38-780, particle volume fractions less than 0.01% and rms turbulent fluctuations due to turbulence generation in the range 0.1-10.0% of the mean velocity differences between the particles and the continuous phase. Instantaneous velocity records showed affects of particle wake disturbances in the streamwise direction but were more dominated by inter-wake turbulence in the crosstream direction; peaked probability density functions of streamwise velocities and near Gaussian probability density functions of crosstream velocities supported this behavior. The instantaneous velocity records also showed that particle wake properties corresponded to recent observations of laminar-like turbulent wakes for spheres at intermediate Reynolds numbers in turbulent environments. Streamwise velocity fluctuations were correlated reasonably well by assuming that particle wake properties dominated flow properties using a stochastic theory; in contrast, crosstream velocity fluctuations were mainly dominated by inter-wake turbulence due to the weak direct contribution of the particle wakes to the properties of this flow direction. The temporal power spectra of streamwise and crosstream velocity fluctuations exhibited prominent -1 and -5/3 power decay regions associated with contributions from mean velocities in the particle wakes and from particle-wake and inter-wake turbulence, respectively. Finally, streamwise and crosstream integral scales were crudely correlated as functions of the known dissipation rate of the turbulence kinetic energy of the flow.

Nomenclature

C_D	=	sphere drag coefficient
C_u, C_v	=	coefficients of velocity fluc-tuation correlations, Eq. (7)
C_u' C_v'	=	coeffecients of integral length scale correlations, Eq.(9)
D	=	dissipation factor, Eq. (8)
d_p	=	sphere diameter
$E_u(f), E_n(f)$	=	streamwise and crosstream temporal power spectra
f	=	frequency
f_w	=	wake volume fraction
G^{-2}	=	mean-squared effect due to particles of diameter d_p
g, g'	=	mean and fluctuating effects at a point due to an individual particle
k	=	turbulence kinetic energy
L_u, L_v	=	streamwise and crosstream integral length scales
ℓ	=	characteristic wake width, Eq. (6)
ℓ_k	=	Kolmogorov length scale
ℓ_p	=	mean particle spacing
n_u, n_v	=	powers of integral length scale correlations, Eq.(7)
$\dot{n}''$	=	particle number flux
PDF	=	probability density functions of streamwise or crosstream velocities.
Re, Re_t	=	particle laminar and turbulence Reynolds numbers, $d_p U_p/\nu$ and $d_p U_p/\nu_t$
r	=	radial distance
t	=	time
t_k	=	Kolmogorov time scale

U_p	=	mean streamwise relative velocity of particle
$\bar{u}$	=	mean streamwise air velocity
$\bar{u}'$	=	rms fluctuating streamwise air velocity
u_k	=	Kolmogorov velocity scale
$\bar{v}$	=	mean crosstream air velocity
$\bar{v}'$	=	rms fluctuating crosstream air velocity
x	=	streamwise distance
ε	=	rate of dissipation of turbu-lence kinetic energy
θ	=	wake momentum diameter, $(C_D d_p^2/8)^{1/2}$
ν, ν_t	=	molecular and turbulent kinematic viscosities
τ	=	temporal integral time scale
ϕ	=	azimuthal angle

Subscripts

c	=	centerline value
o	=	virtual origin condition
∞	=	ambient condition

Introduction

A study the modification of continuous-phase turbulence properties due to the presence and motion of a dispersed phase is described. Hinze[1] identifies several turbulence modification mechanisms that are observed in dispersed flows. Of these, the least understood turbulence modification mechanisms involve direct effects of dispersed phases on continuous-phase turbulence properties, as follows: (1) the exchange of kinetic energy between the dispersed and continuous phases as the dispersed-phase motion accommodates to the continuous-phase motion, denoted turbulence modulation,[2-5] which generally decreases turbulence fluctuations; and (2) the direct disturbance of the continuous-phase velocity field by particle wakes, denoted turbulence generation, [4-8] which generally increases turbulence fluctuations. Evaluating the relative magnitude of these two effects to determine whether turbulence modification will increase or decrease turbulence levels has been addressed during a number of past investigations.[3, 9-12] Although specific criteria differ, these studies show that turbulence generation (modulation) dominates effects of turbulence modification, tending to increase (reduce) turbulence levels, when dispersed-phase elements have large (small) relaxation times compared to characteristic turbulence time scales. As a result, turbulence generation tends to dominate

turbulence modification in many practical dispersed flows when separated-flow effects are significant (e.g., sprays, particle-laden jets, bubbly jets and rainstorms, among others)[2]. Thus, the present study addresses turbulence generation in review of its importance to practical applications.

Past studies of turbulence generation have considered dilute dispersed flows in both shear flow[4-6, 12] and homogeneous flow, [7,8,13] configurations; however, the latter offer the most tractable experimental configuration because they avoid problems of separating effects of turbulence generation from mechanisms of continuous-phase turbulence production in shear flows.[2] One of the first studies along these lines was Lance and Bataille[13] who considered homogeneous air/water bubbly flows downstream of a turbulence-generating grid. Effects of turbulence generation caused a progressive increase of continuous-phase turbulence levels with increasing void fractions; unfortunately, these results still are difficult to interpret due to combined effects of bubble-and grid-generated turbulence.

Earlier work in this laboratory considered homogeneous flows where turbulence generation was the only mechanism of turbulence production.[7,8] These studies involved uniform number fluxes of nearly monodisperse round glass beads falling at their terminal velocities in nearly stagnant (in the mean) water and air. Measurements included phase velocities and turbulence properties for various particle sizes (to provide intermediate particle Reynolds numbers of 100-800 which is typical of practical dispersed flows such as sprays[2]) and particle number fluxes. The flows were analyzed using a simplified stochastic method involving superposition of randomly-arriving particle velocity fields, by extending the method Rice[14] used to analyze noise. The stochastic approach provided some useful interpretations of flow properties, however, the analysis was not definitive because information about particle wakes at intermediate Reynolds numbers in turbulent environments typical of homogenous dispersed flows was limited.[7,8] Thus, it was necessary to estimate wake properties by extrapolating available results at large Reynolds numbers in nonturbulent environments, which is questionable and caused convergence problems of the Rice[14] approach similar to those encountered during stochastic analysis of sedimentation.[15] Other difficulties of these studies involved the

nearly stagnant (in the mean) continuous phases which caused significant experimental uncertainties due to the very large turbulence intensities of the flows (up to 1000%), and potential modification of flow properties due to buoyant disturbances.

Subsequently, several studies of sphere wakes at intermediate Reynolds numbers in both nonturbulent and turbulent environments were undertaken in order to provide information needed to better understand turbulence generation.[16-18] Wakes in nonturbulent environments yielded anticipated behavior for self-preserving turbulent and laminar wakes,[19,20] with transition between these flows at wake Reynolds numbers on the order of unity.[16] Findings more relevant to turbulence generation involved sphere wakes at intermediate Reynolds numbers in turbulent environments which showed that these wakes scaled in the same manner as self-preserving laminar wakes but with significantly enhanced viscosities due to the presence of turbulence (termed "laminar-like turbulent wakes").[17,18] Naturally, the properties of laminar-like turbulent wakes differed substantially from the wake properties assumed in the earlier turbulence generation studies[7,8] implying that these stochastic predictions must be revised.

In summary, review of past work has highlighted deficiencies of both earlier measurements and analysis of turbulence generation phenomena, even for the relatively simple and fundamental stationary homogenous dispersed-flow configuration. Thus, the objectives of the present investigation were to extend Refs. 7 and 8, as follows: (1) to complete new measurements of stationary homogenous dispersed flows involving nearly monodisperse spherical solid (glass) particles at intermediate Reynolds numbers in air, using a counterflow particle/air wind tunnel flow, and (2) to analyze these flows by extending the earlier stochastic analysis to consider the properties of laminar-like turbulent wakes.

The paper begins with discussions of experimental and theoretical methods. Results are then described considering apparatus evaluation, particle wake properties, and continuous-phase properties, in turn. The paper ends with a summary of the major conclusions of the study.

Experimental Methods

Apparatus

A sketch of the experimental apparatus appears in Fig. 1. The configuration involves a vertical counterflow wind tunnel with upflowing air moving toward the suction side of a blower and freely-falling particles introduced using a particle feeder. The measurements were made in a windowed test section located between the air inlet and the particle distribution systems. The particles consisted of nearly monodisperse glass beads having nominal diameters of 0.5, 1.1 and 2.2 mm.

The air flow system consisted of a rounded inlet, a honeycomb flow straightener (10 mm hexagonal cells having a length of 76 mm), and a 16:1 area ratio contraction to the 305 × 305 mm crossection test section that was 1920 mm long. The test section was windowed over its whole length with removable side walls to facilitate the installation of probes and calibration equipment. The test section was followed by a 2390 mm long particle dispersion section. The upper part of this section (1170 mm long) involved an array of 9 equally-spaced screens consisting of stainless steel wire mesh cloth in a square pattern with 0.89 mm diameter wires spaced 4.2 mm apart. The particle inlet section and the transition section to the blower followed the particle dispersion section and had a total length of 1270 mm. The wind tunnel air flow was provided by a single-inlet variable speed blower having an SCR speed controller and a maximum flow rate of 30 cu-m/min. The exhaust from this blower was collected by the laboratory exhaust system in order to prevent buildup of laser velocimetry seeding particles within the test area.

The particle flow was provided by a variable-speed screw feeder (Accurate, model 310 having a 25 mm diameter helix with a center rod for the 0.5 mm diameter particles and a 19 mm diameter helix with a center rod for the 1.1 and 2.2 mm diameter particles. After passing through the wind tunnel, the particles impacted on a plastic sheet within a particle collector. Microscope inspection showed that the particles were not chipped or otherwise damaged when passing through the counterflow wind tunnel; therefore, they were re-used.

Instrumentation

Measurements included particle number fluxes, gas velocities and particle velocities; however, the particle velocities are not reported here and these measurements are not discussed in the following. Particle number fluxes were measured by collecting particles in a thin-walled cylindrical container having a diameter of 25 mm that was closed at the bottom. The container was mounted on a rod so that it could be traversed over the crossection of test section. The experimental uncertainties of these measurements were dominated by finite sampling times which were selected to keep uncertainties (95% confidence) less than 10%.

Gas and particle velocities were measured using laser velocimetry. The plane of the optical measurements was 3500-4500 mm above the floor of the test area while the counterflow wind tunnel was not movable; therefore, provision was made to traverse the laser-velocimetry system. The present traversing system included a heavy-duty milling machine base that provided vertical and lengthwise (along the optical axis) adjustment, a rigid support frame and an optical breadboard mounted on the support frame using linear bearings and a stepping-motor driven linear positioner (Velmex, Model. MA4015K1-S4, with a 5 μm positioning accuracy). The laser velocimeter measurements were based on the 514.5 nm line of an argon-ion laser having an optical power of 1900 mW; this laser was mounted permanently on a fixed table with the laser signals sent to the optical system using a fiber optic link.

The gas velocity measurements were made using single-channel dual-beam, forward-scatter, frequency-shifted laser velocimetry. Streamwise and crosstream velocities were measured by rotating the optics accordingly. The sending optics included a 3.75:1 beam expander that yielded a measuring volume having a diameter of 55 μm and a length of 420 μm. Due to the small measuring volume, the frequency of test particles passing through the measuring volume was very small; in any event, the test particles were readily detected due to their large signal amplitudes and velocities compared to the gas flow so that such data could be eliminated from the data set that was processed to find gas velocities. The air flow entering the wind tunnel was seeded with oil drops (1 μm nominal diameter) using several multiple-jet seeders. Velocities were found from the low-pass filtered analog output of a burst-counter signal processor. Data were collected using a 16-bit analog/digital converter operating at a frequency comparable to the data rate with the break frequency of the filter set at one-half the sampling rate to control alias signals. The combination of frequency shifting plus a constant sampling rate of the analog output eliminated effects of directional bias and ambiguity and velocity bias. Sampling periods were adjusted to provide the following experimental uncertainties (95% confidence): mean velocities less than 5%, rms velocity fluctuations less than 10%, probability density functions within one standard deviation of the most probable velocity less than 10% and temporal power spectral densities less than 20% (at frequencies smaller than the reciprocal of the temporal integral scale with uncertainties smaller elsewhere). All measurements were repeatable within these ranges over a period of testing of several months.

Test Conditions

The properties of the spherical test particles are summarized in Table 1. The particles were nearly monodisperse with standard deviations of particle diameters less than 10% of their nominal diameters. Relative particle velocities were 3-5 times larger than the upflow velocities, while the relative turbulence intensities of the continuous phase were less than 5%; therefore, laser velocimetry measuring conditions were excellent. Particle Reynolds numbers were in the range 100-800, which is representative of the intermediate Reynolds number conditions of drops in sprays.[2,16] Drag coefficients and wake momentum diameters agreed within 15% of values for solid spheres due to Putnam[21] as follows:

$$C_D = 24(1 + Re^{2/3}/6)/Re \qquad (1)$$

The ranges of test variables during the present investigation were somewhat larger than Mizukami et al.;[8] they are summarized in Table 2. Given the mean particle number flux and the absolute velocity of the particles at the near terminal velocity conditions where the present observations were made, the mean particle spacing can be found from

$$\ell_p = ((u_p - \bar{u})/\dot{n}'')^{1/3} \qquad (2)$$

4

assuming that the particles are falling randomly. Based on Eq. (2) present values of mean particle spacing were in the range 13-208 mm which implies particle volume fractions < 0.003%. Based on earlier work,[3] particle velocity fluctuations are negligible due to modest air velocity fluctuations and poor particle response to air motion. For such conditions, the rate of dissipation of turbulence kinetic energy in the measuring region can be equated to the rate of generation of turbulence by particles, which in turn is equal to the rate of transfer of mechanical energy to the gas as the particles move through the flow; i.e.

$$\varepsilon = \pi \dot{n}'' d_p^2 C_D U_p^2 / 8 \qquad (3)$$

The ranges of dissipation rates for present tests are summarized in Table 2. For these conditions, direct dissipation by particles was less than 2% of the continuous-phase dissipation rates; therefore, the present flows were properly dominated by turbulence generation. Given the rate of dissipation of turbulence kinetic energy, the Kolmogorov scales can be computed yielding the ranges summarized in Table 2. Relative turbulence intensities of the flow due to turbulence generation spanned nearly two orders of magnitude and were in the range 0.18-5.03%. Finally, the volume fractions of the wakes (based on wake volumes contained in radial scales of 2ℓ and having a streamwise length where $\bar{u}_0 / \bar{u}' = 0.3$ were less than 19%.

Theoretical Methods

Stochastic Analysis

The qualitative features of turbulence generation in dispersed flows are sketched in Fig. 2 in order to help define the stochastic analysis used to interpret the measurements. As shown, the flow consists of particles with significant wake disturbances associated with each particle. The wake disturbances decay in both the streamwise and crosstream directions and they eventually merge with the inter-wake turbulence field. For present conditions, particle volume fractions are small, less than 0.003%, so that the region near the particle is small and can be ignored compared to the self-preserving region of the wakes. In addition, wake volume fractions are generally small as noted in Table 2; therefore, the probability that two wakes

cross each other, or interact directly, is also relatively small. Thus, the flow is assumed to consist of particle wakes in a turbulent environment, having the properties of laminar-like turbulent wakes defined by Wu and Faeth, [17,18] separated by a homogeneous inter-wake turbulence field. The specific nature of the homogeneous inter-wake turbulence field is not known but analogous to grid-generated turbulence (which also lies outside the region where there are significant wake disturbances due to the grid elements) it seems plausible that this region approximates an isotropic turbulence field. Particle and particle-wake arrival times at a point are random, however, which complicates the separation of flow properties into contributions from the wakes and from the inter-wake turbulence field.

The simplified stochastic analysis of Parthasarathy and Faeth[7] was used to help interpret and correlate a portion of the measurements. The major assumptions of this analysis are as follows: the flows are statistically stationary with uniform particle fluxes and constant continuous-phase properties; mean particle fluxes in the crosstream direction are uniform while particle arrival times at a point satisfy Poisson statistics, i.e., they are independent of other particle arrival times; the flows are infinite in extent which is justified because measured flow properties did not vary appreciably in either the streamwise or crosstream directions; the flows are dilute so that the probability of a test point being within a particle, or in the near wake region of a particle, is negligibly small; because the flows are dilute, the probability of two wakes interacting is also small so that wake properties can be described laminar-like turbulent wake behavior of Refs. 17 and 18; and finally the direct contributions of inter-wake turbulence to flow properties are ignored. Present measurements will suggest that many flow properties involve significant contributions from both the wakes and the inter-wake turbulence field; thus, the last approximation is mainly used to provide a basis for identifying the effects of these two contributions.

Summing flow properties under these assumptions is done by extending methods used to analyze random noise due to Rice.[14] Let the point of observation be the origin of a cylindrical coordinate system with x being the streamwise direction and r and ϕ the radial and azimuthal coordinates. Considering the potential effects of

wake unsteadiness, or turbulence, the arrival of a particle at $x = 0, r, \phi$ and time $t=0$ can produce effects $g(r, \phi, t)$ and $g'(r, \phi, t)$ at the point of observation due to mean and fluctuating (turbulent) wake properties. Following Rice[14], Campbell's theorem can be extended to treat random arrivals of particles over a plane as a summation of effects of individual particles.[18] This yields the following expression for the mean-squared fluctuation about the average for monodisperse particles:

$$G'^2 = \dot{n}'' \int_{-\infty}^{\infty} dt \int_{0}^{2\pi} d\phi \int_{0}^{\infty} (g^2(r,\phi,t) + g'^2(r,\phi,t))r\,dr \qquad (4)$$

see Ref. 7 for corresponding expressions for the time-averaged effect and the generalization of these expressions to treat polydisperse particle flows. Naturally, a further requirement for the proper use of Eq. (4) is that the integrals must converge. Finally, in order to estimate G'^2, expressions are needed for the particle wake effects, g and g', these results are considered next for laminar-like turbulent wakes.

Sphere Wake Properties

Mean streamwise velocities in laminar-like turbulent wakes can be correlated according to the classical similarity analysis of self-preserving round laminar wakes having a constant viscosity, as follows:[17,18]

$$32\,\bar{u}(x-x_0)/(Re_t d_p U_p C_D) = \exp(-r^2/2\ell^2) \qquad (5)$$

where $\bar{u}$ and U_p are taken relative to any ambient mean streamwise velocity in Eq. (5) while $\bar{V}/U_p$ can be found from Eq. (5) using the governing equation for mean conservation of mass. The characteristic wake width, ℓ, in Eq. (5) is given by

$$\ell/d_p = (2(x-x_0)/(d_p Re_t))^{1/2} \qquad (6)$$

while correlations v_t/v in terms of Re and $\bar{u}'/U_p$ can be found in Refs. 17 and 18. Past measurements show that the laminar-like wake region extends from the near-wake region, $(x-x_0)/d_p > 2$, up to conditions where the maximum mean streamwise wake velocities are comparable to ambient velocity fluctuations. Beyond this condition, a fast-decay wake region is observed, where mean streamwise wake velocities decay more

rapidly than the first power of $(x-x_0)/d_p$; this assures the convergence of the integrals of Eq. (4), and the applicability of Campbell's theorem to turbulence generation. The effect of the fast-decay region on turbulence generation properties was small; therefore, the integrations of Eq. (4) were simply terminated at $\bar{u}_c/\bar{u}_\infty' = 0.3$, noting that use of other criteria in the fast-decay wake region had little effect on predictions.

Similar to turbulent wakes in nonturbulent environments,[16] velocity fluctuations in laminar-like turbulent wakes are large, approaching U_p in the near-wake region, for Re >100.[17,18] Thus, wake velocity fluctuations were considered when evaluating Eq. (4). The necessary plots and tabulations of rms streamwise and crosstream velocity fluctuations are presented for various Re and $\bar{u}_\infty'/U_p$ in Refs. 17 and 18.

Using the laminar-like turbulent wake properties in Eq. (4) as just described, suggests a simple correlation of streamwise and crosstream velocity fluctuations, as follows:

$$\bar{u}'/U_p = C_u\,D^{n_u} \qquad (7a)$$

and
$$\bar{V}'/U_p = C_v\,D^{n_v} \qquad (7b)$$

where the parameters C_u, C_v, n_u and n_v take on the best fit values summarized in Table 3. The dimensionless dissipation factor appearing in Eq. (7) is defined as follows:[7,8]

$$D = \varepsilon d_p(\theta/d_p)^2/U_p^3 \qquad (8)$$

all the parameters in Eqs. (7) and (8) are known for a particular particle flux and size, providing a simple way to find rms velocity fluctuations due to turbulence generation in homogeneous dispersed flows.

Results and Discussions

Apparatus Evaluation

The main issues concerning evaluation of the apparatus was to determine whether the dispersed-and continuous-phase flows where properly stationary and homogeneous, and that velocity fluctuations were due to effects of turbulence generation rather than disturbances of the wind tunnel flow. The temporal and spatial

6

uniformity of the particle flows were evaluated by traversing the sampling probe along the two perpendicular axes of symmetry at the lowest crossection where measurements were made. These measurements were carried out for all three particle sizes considered, spanning the ranges of particle fluxes for each size. Samples obtained from multiples of the shortest sampling period showed that the particle fluxes were statistically stationary. Finally, the sampling measurements showed that mean particle fluxes varied less than 10% over the central 205 × 205 mm crossection of the flow where corresponding continuous-phase velocity measurements could be made. Thus, particle properties were adequately stationary and homogenous.

The properties of the gas phase were mainly established by measurements of mean and fluctuating streamwise velocities over the central 205 × 205 mm crossection of the flow, considering streamwise distances up to ± 100 mm from the normal crossection where measurements were made. The results of these measurements did not vary significantly with upflow velocities in the range 500-2000 mm/s. For these conditions, the present flows were statistically stationary and homogeneous within experimental uncertainties, i.e., within 5% for mean velocities and within 10% for velocity fluctuations.

*Measurements of streamwise velocities for various particle sizes, particle fluxes and upflow velocities, were also used to establish minimum allowable particle fluxes. In particular, very low particle fluxes for a given upflow velocity yielded rather large relative turbulence intensities. This behavior was caused by thermal disturbances associated with the large vertical height of the apparatus. Increasing the particle flux, however, disrupted the thermal disturbances and caused relative turbulence intensities to decrease for a time as particle fluxes increased before increasing once again in a manner similar to the observations of Refs. 7 and 8. Thus, present measurements were only undertaken for particle fluxes greater than the minimum relative turbulence intensity condition. Relative turbulence intensities at low particle fluxes were also affected by the upflow velocity. Upflow velocities of 1.0-1.1 m/s were finally selected in order to maximize the range of particle fluxes that could be considered while avoiding the excessive particle concentrations in the flow that

are observed when upflow velocities approach the terminal velocity of the particles, see Eq. (2).

Particle Wake Properties

Given satisfactory evaluation of the apparatus, experiments turned to direct observation of flow velocities for various particle sizes and fluxes. The objectives of these measurements were to identify the direct contributions of particle wakes to gas-phase flow properties, and to assess whether mean velocity distributions in the wakes were similar to the past observations of laminar-like turbulent wakes of Refs. 7 and 8.

Typical streamwise and crosstream velocity records in the present stationary and homogeneous dispersed flows are illustrated in Fig. 3. Results are shown for the particles having a nominal diameter of 0.5 mm at high and low loadings; see Table 4 for a summary of these test conditions. In viewing this data it should be recalled that the measurements of streamwise and crosstream velocities are not simultaneous and no correspondence between these two velocity traces for a particular condition should be inferred.

The most obvious features of the velocity signals illustrated in Fig. 3 are that the streamwise velocity signals exhibit large negative spikes, with the frequency of observing spikes increasing with particle loading. In contrast, the crosstream velocity signals do not exhibit spikes but are similar to the appearance of streamwise velocity signals in the time interval between spikes. Finally, longer periods of observation reveal some spikes with negative absolute velocities reaching -2 to -3 m/s; this implies relative velocities in the range 3-4 m/s, which is reasonable for actual range of particle sizes and for these test conditions (see Table 1). Thus, the behavior of the velocity traces illustrated in Fig. 3 is consistent with the spikes resulting from the direct velocity disturbances of particle wakes. Naturally, increasing numbers of spikes with increasing particle fluxes, and maximum observed relative velocities comparable to the terminal velocities of the particles, are obvious properties that the spikes must satisfy. The presence of spike disturbances only in the streamwise velocity component is also consistent with particle wake properties at these conditions. In particular, mean crosstream velocities are always small compared to mean streamwise velocities in

wakes, while direct effects of crosstream wake turbulence are small for Re of 106, see Refs. 17 and 18; therefore, wake velocity disturbances should be limited to the streamwise velocities as long as particle trajectories are reasonably vertical. Taken together, these results suggest that streamwise velocity properties are probably dominated by inter-wake turbulence properties, for the conditions of Fig. 3.

Another issue of interest is whether the wake properties observed in the present flows correspond to the laminar-like turbulent wake properties observed by Wu and Faeth[17,18] for sphere wakes having a variety of ambient turbulence environments. This issue was also addressed using particles having a nominal diameter of 0.5 mm and a relatively large particle flux (the high-loading conditions in Table 4) so that representative particle wakes could be observed in a reasonable test time. These measurements involved observations of streamwise velocities with relatively dense laser-velocimeter seeding levels so that velocity distributions within the narrow spikes seen in Fig. 3 could be observed. Measurements were made for various maximum dimensionless mean velocity defects, which represents results for paths of the laser velocimetry measuring volume at various radial distances from the wake axis. Effects of turbulence were handled by averaging several velocity records to obtain an estimate of mean streamwise wake velocities (the averaging criterion involved an experimental uncertainty (95% confidence) of the maximum mean velocity defect less than 10%). Predictions assuming vertical wake axes and having the same maximum mean dimensionless velocity defects, were obtained for the same conditions as the experiments from the laminar-like turbulent wake results of Refs. 17 and 18.

The resulting measured and predicted mean dimensionless velocity defects are illustrated in Fig. 4. It is evident that the agreement between measurements and predictions is excellent which supports the use of laminar-like turbulent wake properties to help estimate and interpret the behavior of turbulence generation in homogeneous dispersed flows.

Probability Density Functions

More insight about the relative contributions of wake and inter-wake turbulence properties on the total turbulence properties of homogeneous dispersed flows dominated by turbulence generation can be obtained from the probability density functions of velocity fluctuations. Typical results along these lines are presented in Figs. 5-7 for 2.2, 1.1 and 0.5 mm diameter particles, respectively. On each of these plots, PDF's are shown for streamwise and crosstream velocities at the low and high particle loadings specified by dissipation factor values. Fits of the measurements are also shown on the plots, corresponding to least-squares sectional fits for the PDF(u) and best Gaussian fits for the PDF(v).

The present PDF's plotted in Figs. 5-7 are surprising in view of earlier observations of Refs. 7 and 8 for dispersed flows in stagnant baths. In particular, the earlier results yielded Gaussian PDF's for both velocity components, with at most a slight upward bias (roughly 10% when averaged over all test conditions) of the PDF(u) near its most probable value. This behavior agrees with present behavior of PDF(v), which is nicely fitted by Gaussian PDF's for both loadings of all three particle sizes. In contrast, the present PDF(u) are more peaked and somewhat skewed toward negative velocities compared to the mean velocity, i.e., the PDF(u) exhibits greater kurtosis and skewness than the nearly Gaussian PDF(v).[20] In addition, the PDF(u) for each particle size tend to be independent of particle loading, similar to PDF(v), but the PDF(u) became progressively more peaked (or have progressively increasing kurtosis) as the particle size (or Re) decreases. All these characteristics can be explained from the properties of the streamwise and crosstream velocity records (and the spike disturbances due to particle wakes seen in the streamwise velocity record) of Fig. 3, as discussed next.

The main reason for the different PDF(u) of Refs. 7 and 8 and the present study follows from the much improved laser velocimetry conditions of the present study which allowed the near wake region of the spike disturbances due to particle wakes seen in Fig. 3 to be resolved for the streamwise velocity records. This point was easily demonstrated during the present experiments by reducing seeding levels so that the spikes seen in

8

Fig. 3 were rarely resolved; the corresponding PDF(u) then became more Gaussian similar to the results of Refs. 7 and 8. The other properties of PDF(u) and Figs. 5-7 then follow from the well known effects of the properties of the velocity signal on the values of the skewness and kurtosis of the PDF(u). In particular, the spikes always contribute negative velocity signal based on the results illustrated in Fig. 3; this implies a corresponding positive bias of the PDF(u), or positive skewness, based on the well known properties of PDF's.[20] The more rapid reduction of streamwise velocities in the radial direction for small d_p (or Re) conditions (yielding narrower wake disturbance) implies a more peaked PDF(u), or a larger kurtosis of the PDF(u), for similar reasons.[20] In addition, the small effect of particle flux on the PDF(u) and the PDF(v) is consistent with the generally observed behavior of these functions, where the *shape* of the velocity signal as a function of time affects the skewness and kurtosis of the PDF but not the characteristic frequency of the signal,[20] e.g., homogeneous, isotropic dispersed flows have Gaussian PDF's irrespective of their characteristic time or frequency scales. Finally, the absence of discernible spikes for the crosstream velocity record of Fig. 3 is entirely consistent with the Gaussian behavior of the PDF(v). Taken together, the combined findings of Figs. 3 and 5-7 suggest that streamwise velocities contain significant contributions from particle wake disturbances while crosstream velocities contain significant contributions from inter-wake turbulence.

Velocity Fluctuations

Measurements and predictions of streamwise and crosstream relative turbulence intensities are plotted as a function of the dissipation factor, as suggested by Eqs. (7), in Fig. 8. The measurements include the results for particles in a still (in the mean) water bath due to Parthasarathy and Faeth,[7] results for particles in still (in the mean) air due to Mizukami et al.[8] and the present results for particles in counterflowing air. The predictions were completed for the full range of the Reynolds numbers combined during the measurements of laminar-like turbulent wakes (Re of 25-1560,[17,18] which is comparable to the Reynolds number range of the combined measurements illustrated in Fig. 8 (Re of 38-780). On the other hand, the predictions were only

computed for relative turbulence intensities greater than 2% because this is the current lower bound of ambient turbulence intensities for measurements of the properties of laminar-like turbulent wakes, see Refs. 17 and 18; these conditions correspond to the particle/wake flows of Ref. 7 and the upper end of the present test range. The predictions have been extrapolated over the full range of the measurements, however, because earlier computations suggested relatively little effect of the relative turbulence intensity of the correlations of Eq. (7); in addition, such extrapolations were also in general agreement with the available data base.

The various measurements of relative turbulence intensities are in reasonably good agreement with each other. This is particularly true of streamwise turbulence intensities which exhibit relatively little scatter for an order of magnitude variation of particle Reynolds number and roughly a four order of magnitude variation of the dissipation factor. The fit of Eq. (7), with the parameters given in Table 3, is also seen to be quite satisfactory. Notably, the predictions of Eq. (1), in conjunction with the laminar-like turbulent wake properties of Refs. 17 and 18, suggest that n_u and n_v are roughly 1/2; the values listed in Table 3 are not different from this value within the statistical significance of the measurements. The absolute agreement between mean and predicted streamwise relative turbulence intensities is encouraging because the theory really has no adjustable parameters (except for a weak effect of the location where integrations are ended in the fast-decaying portion of the wake, discussed earlier). This supports the idea that streamwise fluctuations are dominated by laminar-like turbulent wake disturbances with the inter-wake region contributing to a relatively small extent, which also agrees with the PDF results illustrated in Figs. 5-7.

The results for crosstream velocities in Fig. 8 are much less satisfactory than the results for streamwise velocities. First of all, while the measurements in particle/water flows of Ref. 7 are well correlated, the particle-air results are much more scattered with present measurements yielding consistently larger values of $\overline{u}'/U_p$ than the rest. This behavior is consistent with the properties of laminar-like turbulent wakes for crosstream velocities where crosstream mean velocities are always small and crosstream velocity fluctuations remain small for Re < 300. This implies much

stronger effects of Re on values of $\bar{V}'/U_p$ from Eq. (4), which is consistent with the observation that values of $\bar{V}'/U_p$ for $d_p = 0.5$ mm (Re = 106) are smaller than the rest for the present measurements. Another factor is the suggestion of the velocity plots of Fig. 3 and the PDF's of Figs. 5-7 that $\bar{V}'/U_p$ should be more dominated by inter-wake turbulence, so that correlations along the lines of Eq. (7) through Eq. (4) are really not to be expected. Finally, some of the scatter observed for $\bar{V}'/U_p$ for the particle/gas flows in Fig. 8 could be caused by particle wakes that are not vertical due to collisions with the walls in the particle dispersion section. Such contributions are feasible due to the relatively brief relaxation times of particle/air flows to terminal velocity conditions (compared to particle/water flows) while even slight contributions from the streamwise velocities of wakes passing at an angle to the vertical could significantly affect observed values of $\bar{V}'/U_p$. Direct measurements of particle velocities, as well as use of a honeycomb particle flow straightener, are currently being undertaken in order to help resolve this issue. In the interim, the predicted correlation of $\bar{V}'/U_p$ illustrated in Fig. 8 should not be considered a definitive assessment of stochastic predictions because this result does not account for either potential effects of particle Reynolds numbers or the vertical alignment of particle trajectories.

Power Spectral Densities

Measured normalized temporal power spectral densities in the streamwise and crosstream directions are plotted as a function of normalized frequency in Figs. 9 and 10. Results are shown for various loadings with test properties for the low and high loadings summarized in Table 4. The actual temporal spectra, and temporal integral scales, depend on $\bar{u}$ through Taylor's hypothesis, and have no fundamental significance; nevertheless, $\bar{u}$ was essentially the same (1.0-1.1 m/s) for present test conditions so that the results can be consistently compared. Laser velocimetry measuring conditions were reasonably good for the present results so that effects of step noise were deferred until Kolmogorov frequencies were approached, i.e., $f\tau \approx \tau/t_k$ where the plots are terminated in Figs. 9 and 10. Finally, the values of τ were found by setting $E_u(f)/(\bar{u}'^2\tau) = 4$ where $f\tau$ becomes small, as discussed by Hinze.[22]

Streamwise power spectral densities provide a reasonable correlation in terms of the normalized variables of Fig. 9 Interesting features of these results involve the prominent -1 and -5/3 power decay regions as $f\tau$ increases. The -1 power decay region is not seen in more conventional turbulent flows; it is due to contributions of mean velocities in particle wakes at relatively low frequencies, which correspond to wake passing frequencies, i.e., the reciprocal of the time required for the entire wake disturbance to pass the measuring location. In particular, wake passing times are roughly 50 ms for the high flux condition illustrated in Fig. 4 for 0.5 mm diameter particles, which is comparable to the integral time scale for this condition appearing in Table 4. This implies dimensionless wake passing frequencies, $f\tau$, on the order of unity which corresponds to the -1 power decay region seen in Fig. 9 This contribution is present in the velocity signal because the arrival times of particle wakes are random so that effects of wake mean velocities cannot be separated from other random turbulence properties. Higher frequencies involve a -5/3 power decay region which should be representative of turbulence in both the wakes and the inter-wake region, as Kolmogorov scales are approached.

The normalized crosstream power spectral densities illustrated in Fig. 10 are more scattered than the corresponding streamwise power spectral densities illustrated in Fig. 9. The apparent scatter near the origin is expected because this spectrum is associated with the correlation of crosstream velocities in the streamwise direction, and reaches a maximum at a finite value of $f\tau$ rather than the behavior of $E_u(f)$ which reaches a maximum as $f\tau$ becomes small. This contribution is present in the velocity signal because the arrival times of particle wakes are random so that effects of wake mean velocities cannot be separated from other random turbulence properties, see Tennekes and Lumley.[20] This spectrum also has -1 and -5/3 power decay regions, the former at frequency ranges associated with mean wake velocity distributions and the latter associated with higher frequency turbulence contributions, as just discussed. The reduced turbulence contribution for crosstream velocity fluctuations at low particle Reynolds numbers is also evident, e.g., crosstream wake turbulence is weak for Re < 300 which does correspond to the more rapid decay of E_v for $d_p = 0.5$ mm seen in Fig. 10. This variation of wake turbulence with Re contributes to the scatter of the normalized spectra

10

at large frequencies. Effects of inter-wake turbulence are no doubt important as well but are difficult to resolve pending conditional measurements to separate contributions from particle wakes and inter-wake turbulence.

Integral Scales

Spatial integral scales are more representative of fundamental flow properties than temporal integral scales which vary with the arbitrary selection of the upflow mean velocity, $\bar{u}$. Thus, spatial integral scales, L_u and L_v, were found from the temporal integral scales using Taylor's hypothesis. Integral length scales probably involve contributions from both particle wakes and inter-wake turbulence which will involve decomposition of flow properties into these two components for a rational treatment. Finding each conditional properties was beyond the scope of the present investigation; therefore, an approach used by Mizukami et al.[8] was investigated instead as a preliminary step. This involved assuming that spatial integral scales are proportional to dissipation length scales represented in the usual manner, i.e., $-k^{3/2}/\varepsilon$ based on dimensional considerations, where k is the turbulence kinetic energy. Then noting that streamwise and crosstream velocity fluctuations scale in the same manner from Eqs. (7), integral length scales should vary as follows:[8]

$$L_u \varepsilon/U_p^3 = C_u' \, D^{n_u'}, \qquad (9a)$$

$$L_v \varepsilon/U_p^3 = C_v' \, D^{n_v'} \qquad (9b)$$

where theory suggests that $n_u' = n_v' = 3/2$.

Measured integral length scales in the streamwise and crosstream directions, for both particle/water and particle/air flows, are illustrated in Figs. 11 and 12. The figures involve dimensionless integral length scales plotted as a function of the dissipation factor as suggested by Eqs. (9). The values of C_u' C_v', n_u' and n_v' of the empirical fits of the measurements shown on these plots are summarized in Table 5; similar to the observations of Mizukami et al.,[8] the fitted powers of D are generally smaller than the value of 3/2 suggested by the theory. The scatter of the measurements about the correlations of Eqs. (9) is rather large. Thus, this approach should only be considered as a tentative first step, pending the

development of more rational methods that properly separate the length-scale contributions of the particle wakes and the inter-wake turbulence field.

Conclusions

This investigation considered the properties of homogeneous turbulence generated by uniform fluxes of monodisperse spherical particles moving through air at normal temperature and pressure. The specific configuration involved particles falling in counterflowing air to supplement earlier findings for particles falling in stagnant water and air. The combined data base involved the following conditions: particle Reynolds numbers of 38-780, particle volume fractions less than 0.01% and particle relative turbulence intensities of 0.1-10.0%. The major conclusions of the study are as follows.

1. The streamwise velocity records exhibited large spikes due to disturbances from particle wakes while the crosstream velocity records yielded only irregular turbulent-like traces with no evidence of disturbances from particle wakes. This behavior suggests that the present flows consist of regions of wake disturbances separated by turbulent inter-wake regions with each region contributing differently to overall flow properties.

2. Instantaneous measurements of gas velocities indicate that the particle wake properties of the present flows corresponded to the laminar-like turbulent wakes observed for spheres at similar intermediate Reynolds number conditions in turbulent environments.

3. The probability density functions of streamwise and crosstream velocities differed from the earlier findings of Refs. 7 and 8 because the velocity disturbances from particle wakes were resolved better during the present study. Thus, the present probability density functions of crosstream velocities were Gaussian while the probability density functions of streamwise velocities exhibited larger values of skewness and kurtosis due to the wake disturbances; in contrast, the earlier measurements reported Gaussian probability density functions for both components of velocity.

4. Streamwise velocity fluctuations were dominated by effects of particle wake disturbances and were correlated quite well by the dissipation

11

factor of the flow based on predictions of stochastic theory; this behavior was supported by the presence of peaked and skewed probability density functions of streamwise velocities that were mentioned earlier.

5. Crosstream velocity fluctuations were dominated by effects of inter-wake turbulence due to the relatively weak direct contribution of wake disturbances to velocity fluctuations in the crosstream direction; this behavior was supported by the Gaussian probability density functions of crosstream velocities mentioned earlier.

6. The temporal power spectra of streamwise and crosstream velocity fluctuations exhibited prominent -1 power decay regions at wake passing frequencies that were associated with contributions from mean velocities in the particle wakes, and prominent -5/3 power decay regions at frequencies extending to the Kolmogorov frequencies due to turbulence in both the wake disturbances and the inter-wake region. The mean velocity distributions of the wake disturbances contributes to the random velocity fluctuations of flow fields resulting from turbulence generation because particle wake arrivals are random and cannot be separated from conventional random turbulent effects.

7. The contribution of mean velocities in the particle wake disturbances is also responsible for the surprisingly large range of scales observed for present flows even though they only involve modest intermediate sphere Reynolds numbers. The streamwise and crosstream integral length scales were crudely correlated in terms of the dissipation factor but improved methods should be sought for these and other properties of flows resulting from turbulence generation by identifying the specific contributions of particle wake disturbances and regions of inter-wake turbulence.

Acknowledgments

References

[1]Hinze, J.O., "Turbulence Fluid and Particle Interaction," Prog. Heat Mass Transfer, Vol. 6, 1972, pp. 433-452.

[2]Faeth, G.M., "Spray Combustion Phenomena," Twenty-Sixth Symposium (International) on Combustion, The Combustion Institute, Pittsburgh, 1996, pp. 1593-1612.

[3]Hetsroni, G., "Particle-Turbulence Interaction," Int. J. Multiphase Flow , Vol. 15, No. 5, 1989, pp. 735-746.

[4]Squires, K.D., and Eaton, J.K., "Particle Response and Turbulence Modification in Isotropic Turbulence," Phys. Fluids A Vol. 2, No. 6,1990, pp. 1191-1203.

[5]Rogers, C.B., and Eaton, J.K, "The Effect of Small Particles on Fluid Turbulence in a Flat-Plate Turbulent Boundary Layer in Air," Physics Fluids A, Vol. 3, No. 5, 1991, pp. 928-937.

[6]Parthasarathy, R.N., and Faeth, G.M., "Structure of Particle-Laden Turbulent Water Jets in Still Water," Int. J. Multiphase Flow, Vol. 13, No. 5, 1987, pp. 699-716.

[7]Parthasarathy, R.N., and Faeth, G.M. "Turbulence Modulation in Homogeneous Dilute Particle-Laden Flows, " J. Fluid Mech., Vol. 220, Pt.2, 1990, pp. 485-514.

[8]Mizukami, M., Parthasarathy, R.N., and Faeth, G.M., "Particle-Generated Turbulence in Homogeneous Dilute Dispersed Flows," Int. J. Multiphase Flow, Vol. 18, No. 2, 1989, pp. 397-412.

[9]Gore, R.A., and Crowe, C.T., "Effect of Particle Size on Modulating Turbulent Intensity," Int. J. Multiphase Flow, Vol. 15, No. 2, 1989, pp. 279-285.

[10]Kenning, V.M., and Crowe, C.T., "On the Effect of Particles on Carrier Phase Turbulence in Gas-Particle Flows," Int. J. Multiphase Flow, Vol. 23, No. 2, 1997, pp. 403-408.

[11]Yuan, Z., and Michaelides, E., "Turbulence Modulation in Particulate Flows — A Theoretical Approach," Int. J. Multiphase Flow, Vol.18, No. 5, 1992, pp. 779-785.

[12]Rashidi, M., Hetsroni, G., and Banerjee, S., "Particle-Turbulence Interaction in a Boundary Layer," Int. J. Multiphase Flow, Vol. 16, No. 6, 1990, pp. 935-949.

[13]Lance, M., and Bataille, J., "Turbulence in the Liquid Phase of a Uniform Bubbly Air-Water Flow," J. Fluid Mech., Vol. 222, Pt. 1, 1991, pp. 95-119.

[14]Rice, S. O., "Mathematical Analysis of Random Noise," Noise and Stochastic Processes (N. Wax, ed.), Dover Publications, New York, 1954, pp. 133-294.

[15]Batchelor, G.K., "Sedimentation in a Dilute Dispersion of Spheres," J. Fluid Mech., Vol. 52, 1971, pp. 245-268.

[16]Wu, J.-S., and Faeth, G.M., "Sphere Wakes in Still Surroundings at Intermediate Reynolds Numbers," AIAA J., Vol. 31, No. 8, 1993, pp. 1448-1455..

[17]Wu, J.-S., and Faeth, G.M., "Sphere Wakes at Moderate Reynolds Numbers in a Turbulent Environment," AIAA J., Vol. 32, No. 3, 1994, pp. 535-541.

[18]Wu, J.-S., and Faeth, G.M., "Effects of Ambient Turbulence Intensity on Sphere Wakes at Intermediate Reynolds Numbers," AIAA J., Vol. 33, No. 1, 1995, pp. 171-173.

[19]Schlichting, H., Boundary Layer Theory, 7th ed., McGraw-Hill, New York, 1979, pp. 234-235 and 599.

[20]Tennekes, H., and Lumley, J.L., A First Course in Turbulence, MIT Press, Cambridge, Massachusetts, 1972, pp. 113-124 and 196-201.

[21]Putnam, A., "Integrable Form of Droplet Drag Coefficient," ARS Journal, Vol. 31, 1961, pp. 1467-1468.

Hinze, J.O., Turbulence, 2nd Ed., McGraw-Hill, New York, 1975, Chapt. 3.

Table 1 Particle properties[a]

Nominal Particle Diameter (mm)	0.5	1.1	2.2
Standard Dev. of Diameter (mm)	0.047	0.11	0.13
Terminal Velocity (mm/s)	3360	4970	5640
Reynolds Number (-)	106	344	780
Drag Coefficient (-)	1.03	0.64	0.47
Wake Momentum Diam. (mm)	0.18	0.28	0.48

[a]Round glass beads (density of 2500 kg/m^3) falling in air at normal temperature and pressure (air density of 1.16 kg/m^3 and kinematic viscosity of 15.9 mm^{2}s). These results are based on the measurements of Parthasaraathy and Faeth[7] and Mizukami et al.[8].

Table 2 Summary of test conditions[a]

Nominal Particle Diameter (mm)	0.5	1.1	2.2
$\dot{n}''$ (kpart/m^{2}s)	71-950	4.2-56	0.5-10
ℓ_p (mm)	32.1-13.5	97.3-41.2	208.3-76.8
ε(m^2/s^3)	0.0812-1.083	0.0315-0.417	0.0143-0.285
ℓ_k (mm)	0.47-0.25	0.60-0.31	0.73-0.35
t_K (ms)	14.0-3.8	22.4-6.2	33.4-7.5
u_K (mm/s)	33.7-64.4	26.6-50.7	21.8-46.2
$\overline{u}/U_p$ (%)	0.52-5.03	0.22-0.90	0.18-0.80
$\overline{v}/U_p$ (%)	0.54-1.28	0.21-1.24	0.20-1.09
f_w (%)	1.89-1.1	12.5-9.3	3.5-3.6

[a]Particle volume fractions < 0.003%; direct dissipation by particles < 2%; actual mean streamwise coflow velocities were in the range 1.0-1.1 m/s.

Table 3 Summary of relative turbulence intensity correlations[a]

Velocity Component	u	v
C_u, C_v	2.21	2.15
n_u, n_v	0.37	0.41

[a]Based on predictions for laminar-like turbulent wakes at large Re where v_t/v is independent of the ambient relative turbulent density.

Table 4 Sample test conditions

Loading	$\dot{n}''$ (kpart/m^{2}s)	$D \times 10^7$ (-)	$\overline{u'}/U_\infty$ (%)	τ (ms)	t_K (ms)
$d_p = 0.5$ mm:					
Low	10.3	1.99	1.0	100.2	11.6
High	635	12.2	3.5	45.4	4.7
$d_p = 1.1$ mm:					
Low	6.0	0.32	0.30	176.0	18.8
High	37.0	1.99	0.77	67.0	7.7
$d_p = 2.2$ mm:					
Low	0.73	0.15	0.19	1290	27.8
High	6.69	2.06	0.66	46.0	9.1

Table 5 Summary of spatial integral length scale
correlations[a]

Velocity Component	u	v
C_u', C_v'	27.8	162
n_u', n_v'	0.74	0.97

[a]Based on best fit of the measurements of
Parthasarathy and Faeth[7], Mizukami et al.[8] and the
present investigation for D in the range 4×10^{-8} - 2
$\times 10^{-4}$.
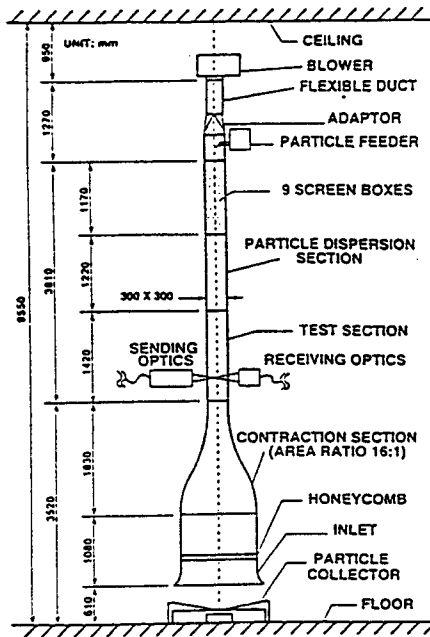
Fig. 1 Sketch of the counterflow particle/air wind tunnel.
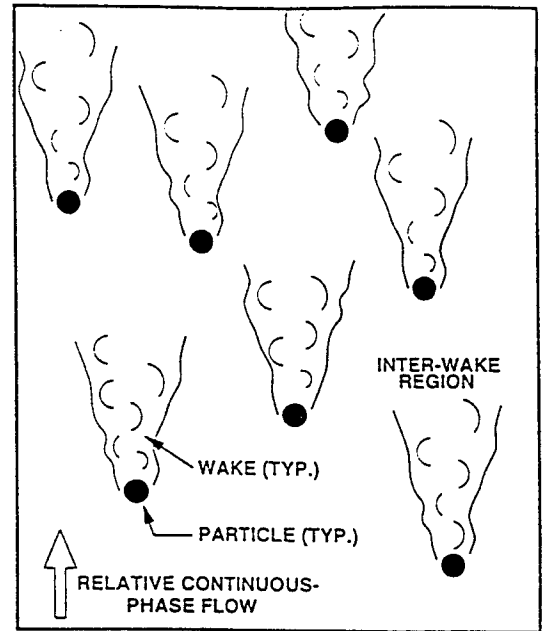
Fig. 2 Sketch of particle-laden dispersed turbulent flow.
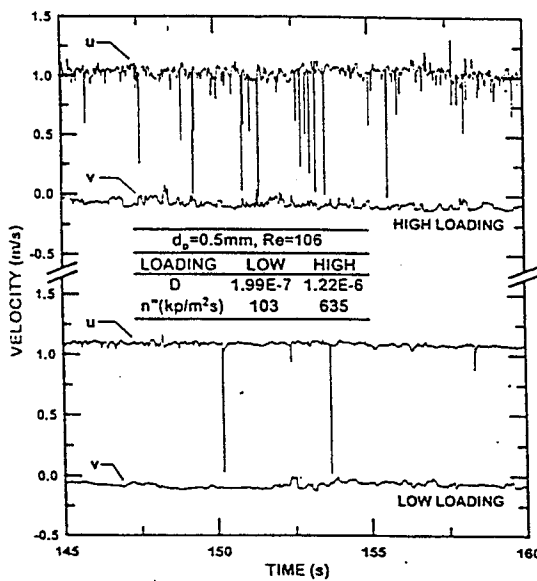
Fig. 3 Streamwise and crosstream velocities as a function of time at high and low particle loadings for 0.5 mm diameter particles.
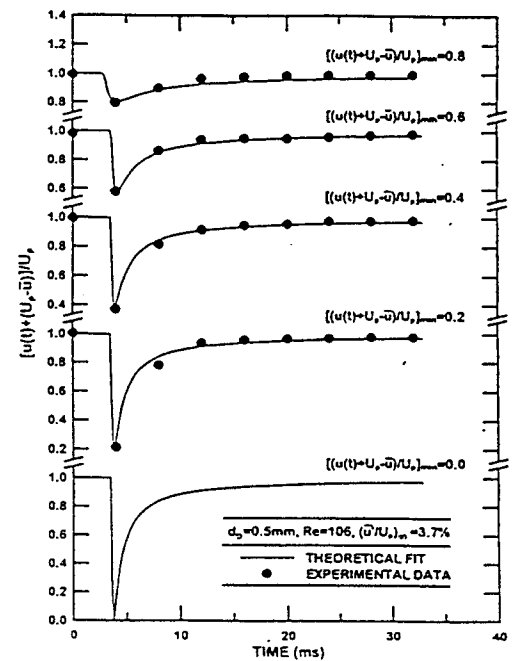
Fig. 4 Measured and predicted streamwise velocities in particle wakes as a function of time for various minimum relative wake velocities.

16
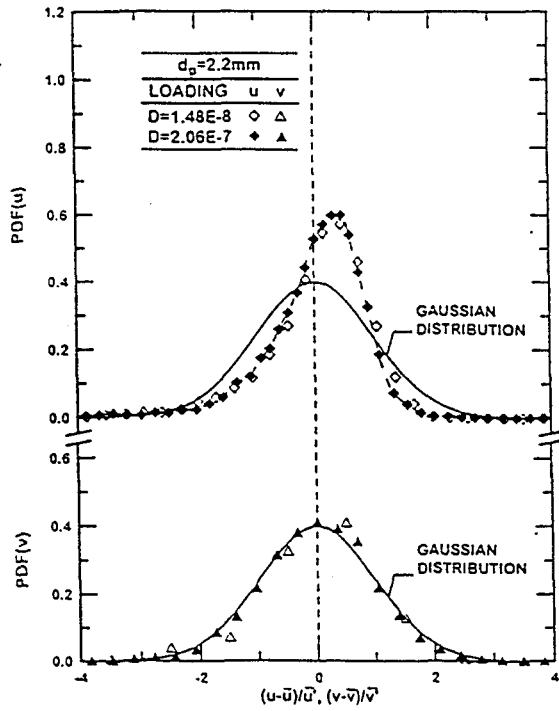
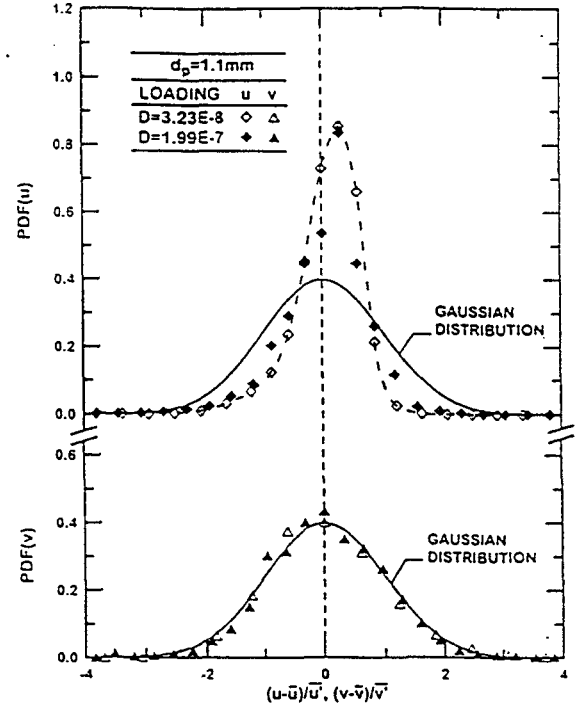Fig. 5 Streamwise and crosstream velocity PDF's at low and high particle loadings for 2.2 mm diameter particles.

Fig. 6 Streamwise and crosstream velocity PDF's at low and high particle loadings for 1.1 mm diameter particles.
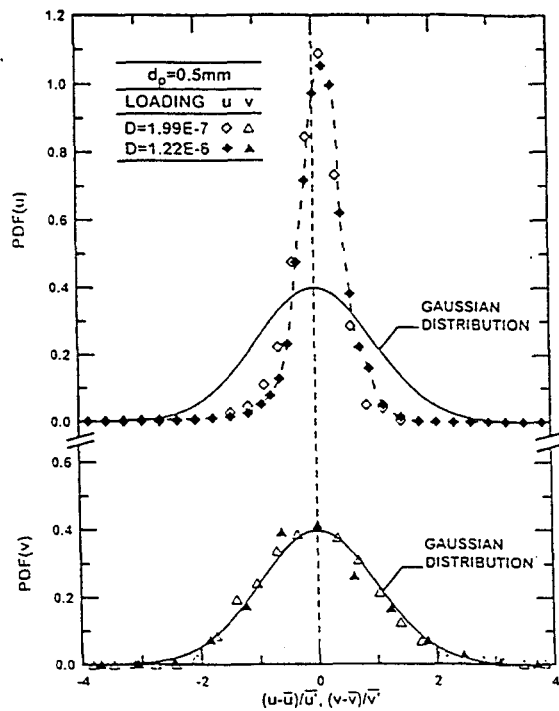
Fig. 7 Streamwise and crosstream velocity PDF's at low and high particle loadings for 0.5 mm diameter particles.
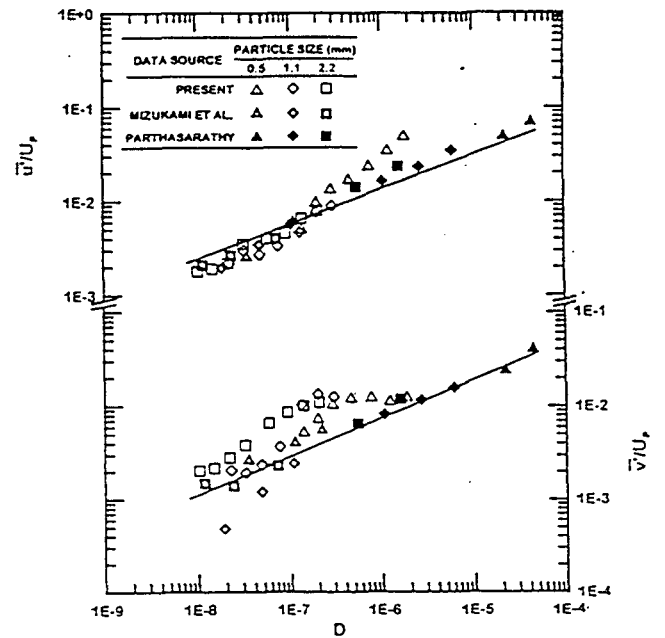
Fig. 8 Streamwise and crosstream r.m.s. velocity fluctuations as a function of particle dissipation rates and diameters.
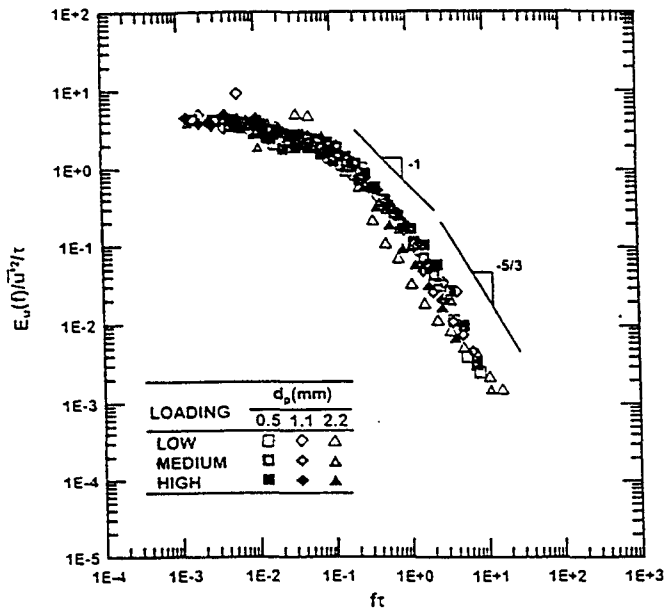
17

Fig. 9 Temporal power spectral densities of streamwise velocity fluctuations for various particle loadings and sizes.
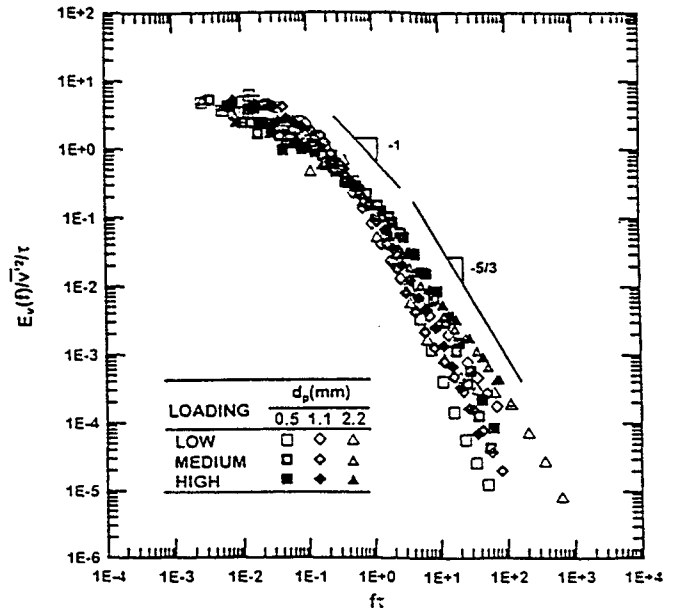

Fig. 10 Temporal power spectral densities of crosstream velocity fluctuations for various particle loadings and sizes.
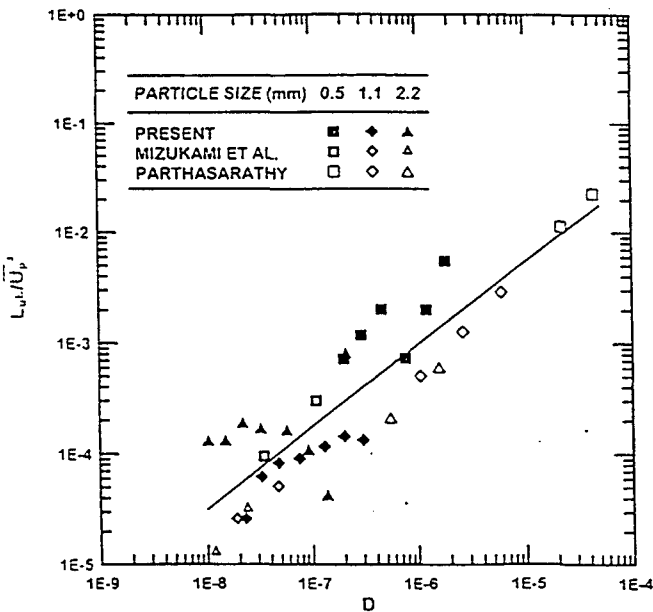

Fig. 11 Streamwise integral length scales as a function of dissipation factor for various particle loadings and sizes.
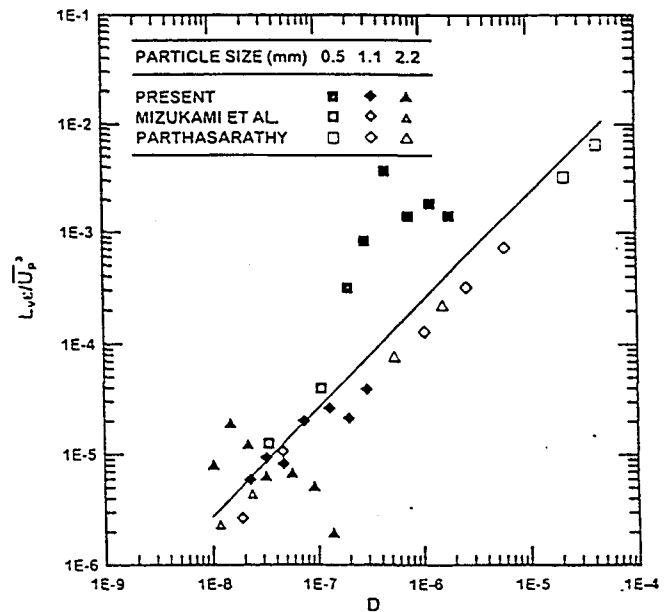

Fig. 12 Crosstream integral length scales as a function of dissipation factor for various particle loadings and sizes.

18